

# RSC Advances



This is an *Accepted Manuscript*, which has been through the Royal Society of Chemistry peer review process and has been accepted for publication.

*Accepted Manuscripts* are published online shortly after acceptance, before technical editing, formatting and proof reading. Using this free service, authors can make their results available to the community, in citable form, before we publish the edited article. This *Accepted Manuscript* will be replaced by the edited, formatted and paginated article as soon as this is available.

You can find more information about *Accepted Manuscripts* in the [Information for Authors](#).

Please note that technical editing may introduce minor changes to the text and/or graphics, which may alter content. The journal's standard [Terms & Conditions](#) and the [Ethical guidelines](#) still apply. In no event shall the Royal Society of Chemistry be held responsible for any errors or omissions in this *Accepted Manuscript* or any consequences arising from the use of any information it contains.

# Structure-Activity Relationship Study of Dendritic Polyglycerolamines for Efficient siRNA Transfection

Fatemeh Sheikhi Mehrabadi,<sup>a</sup> Ole Hirsch,<sup>b</sup> Reiner Zeisig,<sup>c</sup> Paola Posocco,<sup>d</sup> Erik Laurini,<sup>d</sup> Sabrina Prici,<sup>d</sup> Rainer Haag,<sup>a</sup> Wolfgang Kemmner,<sup>e\*</sup> and Marcelo Calderón<sup>a\*</sup>

<sup>a</sup> Institut für Chemie und Biochemie, Freie Universität Berlin, Takustr. 3, 14195 Berlin, Germany

<sup>b</sup> Physikalisch-Technische Bundesanstalt, Abbestr. 2, 10587 Berlin, Germany

<sup>c</sup> Experimental Pharmacology & Oncology GmbH, Robert-Rössle-Str. 10, 13125 Berlin, Germany

<sup>d</sup> Molecular Simulation Engineering (MOSE) Laboratory, DICAMP, University of Trieste, Piazzale Europa 1, 34127 Trieste, Italy

<sup>e</sup> Translational Oncology, Experimental and Clinical Research Center, Charité Campus Buch, Lindenberger Weg 80, 13125 Berlin, Germany

**Abstract** Structure-activity relationship studies are pivotal in the development of existing small interfering RNA (siRNA) nanocarriers and in designing new delivery systems. In this paper, we investigated the ability of four dendritic polyglycerolamines (dPG-NH<sub>2</sub>) with increasing amine degree of functionalization (DF) on dendritic polyglycerol (dPG) to complex DNA by a coupled *in silico/in vitro* approach. In parallel, we examined our dPG-NH<sub>2</sub> analogues for siRNA complexation, cytotoxicity, and transfection efficiency *in vitro* and *in vivo*. Our simulation data indicate the most effective nucleic acid affinities for dPG-NH<sub>2</sub> analogues with DF ≥ 50%. Concomitantly, the results of *in vitro* and *in vivo* transfection studies also demonstrate efficient siRNA transfection only for those dPG-NH<sub>2</sub> analogues with DF ≥ 50%. Thus, both MD simulation and siRNA knockdown studies show that a minimum DF per dPG unit (namely 50% on a 10 kDa dPG) is needed to achieve efficient siRNA interaction and successful transfection.

## Introduction

Post-transcriptional gene silencing by short interfering RNA (siRNA) is a powerful tool for the treatment of various diseases.<sup>1-6</sup> However, the broad application of siRNA-based therapeutics is limited due to the lack of safe and efficient delivery systems. The stability of unmodified siRNA in blood stream is low. Moreover, naked siRNA can be immunogenic and cannot readily cross the cellular membrane to reach the cytoplasm.<sup>7</sup> Besides modified oligonucleotides,<sup>8</sup> a wide range of materials are under development to tackle the problem of *in vivo* siRNA delivery.<sup>9-11</sup> Among diverse materials available to the purpose, polycationic dendrimers based on polyamines are repeatedly employed.<sup>12</sup>

Recently, dendritic polyglycerols (dPGs) have been used by our group in a wide range of applications like antifouling,<sup>13</sup> tissue engineering,<sup>14</sup> and anti-cancer therapy.<sup>15-17</sup> The controlled synthesis of dPG-based scaffolds results in defined structures with relatively precise molecular weights and low dispersity, which, in turn, is reflected in the vast array of possible uses for these compounds. Besides, dPG has numerous hydroxyl end groups that can be appropriately functionalized. Furthermore, the polyether backbone of dPG is fairly stable and inert under biological conditions, and the biocompatibility of this molecule has been proved.<sup>18-20</sup>

The design and optimization of the polymeric siRNA carriers for safe and efficient transfection have been the subject matter of numerous studies.<sup>21-24</sup> In our group, we examined dendritic polyglycerolamine (dPG-NH<sub>2</sub>) 90% (i.e., a 10 kDa dPG with 90% amine degree of functionalization (DF)) for siRNA delivery.<sup>25</sup> dPG-NH<sub>2</sub> 90% has shown efficient knockdown of several proteins such as Lamin, CDC2, and MAPK2 in HeLAS3 cells.<sup>26</sup> Additionally, intratumoral and intravenous administration of dPG-NH<sub>2</sub> 90% into tumor-bearing mice resulted in significant siRNA knockdown.<sup>25, 27</sup> Nevertheless, therapeutic application of this vector is limited due to its cytotoxicity, which heightens at higher concentrations. In another study, dPG-NH<sub>2</sub> analogues with low amine functionalization (DF  $\leq$  30% on a 10 kDa dPG) exhibited lower cytotoxicity than counterparts with  $\geq$  30% amine functionalization in U-937 cells.<sup>28</sup> Furthermore, the *in vitro* tolerability of dPG-NH<sub>2</sub> analogue with moderate amine DF could be improved by introduction of basic amino acid to it.<sup>29</sup> All these results motivated us to investigate further the structure-activity relationship of dPG-NH<sub>2</sub> molecules with various DF with respect to complexation of genetic materials, cytotoxicity, and transfection efficiency. For the purpose, we adopted a combined approach of *in silico/in vitro/in vivo* experiments. Accordingly, we performed extensive atomistic molecular dynamics simulations<sup>30, 31</sup> to study the interactions of newly synthesized dPG-NH<sub>2</sub> analogues featuring different amine DF with a short (21-bp) DNA model, with the aim of understanding the molecular mechanism behind the

nanocarriers/nucleic acid complexation process. Furthermore, we examined the performance of dPG-NH<sub>2</sub> analogues in terms of cytotoxicity and siRNA transfection efficiency *in vitro* and *in vivo*. We then compared the results of our computational study with the results from biological experiments. From MD simulations, we observed that the DF strongly influences the DNA complexation strength of dPG-NH<sub>2</sub> analogues, whereby the molecules featuring a DF higher than 50% were the most effective DNA binders. In agreement with *in silico* prediction, siRNA silencing studies confirmed the required minimum of 50% DF on the dPG scaffold to achieve efficient siRNA knockdown both *in vitro* and *in vivo*.

## Result and discussion

### Synthesis of dPG-NH<sub>2</sub> analogues

Four dPG-NH<sub>2</sub> analogues (based on dPG of 10.6 kDa average *Mw*) with different numbers of amine functional groups per dPG unit were prepared (Figure 1). dPG possess two types of hydroxyl groups for further functionalization. Hydroxyl groups are either located at terminal positions on the surface of dPG unit or in polymer interior region. At low DF ( $\leq 40\%$ ), conversion of vicinal hydroxyl groups located on the surface of dPG is most predominant due to their accessibility. To explore the effect of partial conversion of hydroxyl groups on dPG to amines, dPG-NH<sub>2</sub> analogues with 10% and 30% DF were prepared. Statistically, at a functionalization degree higher than 40% on dPG, the interior hydroxyl groups start to convert into amines. In the case of dPG-NH<sub>2</sub> 50%, most of the vicinal hydroxyl groups were therefore converted to the desired amine groups (Figure 1). Finally, dPG-NH<sub>2</sub> 90% was prepared, where almost all hydroxyl groups on the surface of dPG and the linear groups in the interior of dPG scaffold were fully converted to amines. Accordingly, the effect of dPG amination (partial or full functionalization) on genetic materials complexation, cytotoxicity, and transfection efficiency could be explored.

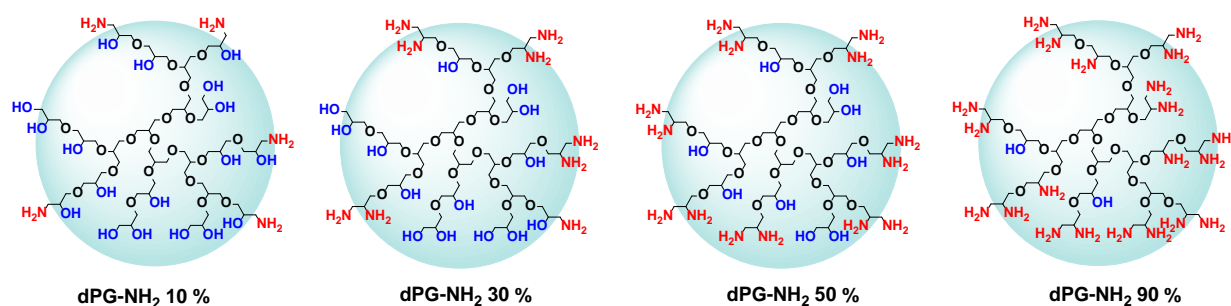


**Figure 1.** Representation of different amine DF in percentage on dPG scaffold. The depicted structure represents only a small idealized fragment of a 10 kDa dPG-NH<sub>2</sub> molecule.

## DNA Binding Studies

To study the binding strength of all synthesized dPG-NH<sub>2</sub> analogues to genetic material, an Ethidium bromide (EthBr) displacement assay was carried out. In this binding study, a 21-bp DNA molecule was used which has shown in previous studies to be an appropriate general model in physicochemical characterization of polyamine polyplexes.<sup>24, 32-34</sup> EthBr is known as an efficient DNA intercalator molecule. As a result of DNA intercalation, fluorescence intensity of EthBr increases. Upon addition of dPG-NH<sub>2</sub> molecules with different amine DF to a mixture of EthBr and DNA, fluorescence decreases in a concentration dependent manner, due to competition between polyamines and EthBr for DNA interaction (Figure 1 in Supporting Information). In this comparative assay a meaningful trend was observed, namely, dPG-NH<sub>2</sub> analogues with DF  $\geq$  50% showed lower CE<sub>50</sub> values than dPG-NH<sub>2</sub> molecules with 10 and 30% DF (Table 1). The CE<sub>50</sub> value represents the necessary “charge excess” to achieve 50% reduction of the relative fluorescence intensity as a result of EthBr displacement. In another words, in the case of dPG-NH<sub>2</sub> 10% and 30%, an almost double value of the amine to phosphate ratio is necessary to achieve the same amount of EthBr displacement obtained with dPG-NH<sub>2</sub> 50% and 90%. Interestingly, however, increasing the DF on dPG from 50 to 90% does not result in any substantial variation of the corresponding CE<sub>50</sub> values. This might have been due to the more productive display of vicinal diamines on dPG with DNA phosphate groups than those amines located in the interior of the dPG scaffold. Thus, not only the DNA binding affinity of dPG-NH<sub>2</sub> analogues strongly depends on their DF but, 50% amination appears to be a critical threshold for amine functionalization to interact with DNA in an efficient way. These results were further confirmed by a gel electrophoresis retardation assay according to which, for highly amine-functionalized dPGs, siRNA was retarded on the gel at lower N/P ratios (N/P  $\geq$  5 for dPG-NH<sub>2</sub> 90%) compared to low-amine functionalized counterparts (N/P  $\geq$  10 for dPG-NH<sub>2</sub> 10%, (Figure 2 in SI).

**Table 1.** Physicochemical properties of dPG-NH<sub>2</sub> analogues.

amine DF % on dPG <sup>a</sup>	amine groups/dPG	$\zeta$ (dPG-NH <sub>2</sub> ) (mV) <sup>b</sup>	Diameter (nm) <sup>c</sup>	PDI <sup>d</sup>	CE <sub>50</sub> (N/P) <sup>e</sup>
dPG-NH <sub>2</sub> 10%	12	8.36 $\pm$ 0.3	6.3	1.33	0.55
dPG-NH <sub>2</sub> 30%	36	9.21 $\pm$ 0.6	8.4	1.29	0.42
dPG-NH <sub>2</sub> 50%	60	13.0 $\pm$ 1.0	9.2	1.27	0.30
dPG-NH <sub>2</sub> 90%	110	14.8 $\pm$ 0.08	14.0	1.30	0.30

<sup>a</sup> Determined by <sup>1</sup>H NMR spectroscopy, <sup>b</sup> measured at pH (7.4), <sup>c</sup> determined by DLS (intensity distributions are reported) <sup>d</sup> Determined by GPC equipped with a RI detector, <sup>e</sup> determined by EthBr displacement assay.

## Modeling Results

To further explore the critical role of amine DF on dPG in the DNA binding process, all polyamines were modeled and simulated employing atomistic molecular dynamics (MD) techniques in aqueous solution (pH 7.4) and in the presence of salt.

From these calculations, an estimation of the average dimension of each dPG-NH<sub>2</sub> molecule was derived as listed in the first row of Table 2. From the values in Table 2 we observe that hydroxyl substitution up to 50% does not result in a significant difference in molecule diameter, which is approximately equal to 4.4 nm. However, when DF is higher than 50%, the presence of a large number of charged groups leads to 25% increase molecular dimensions ( $\Phi = 5.7$  nm), swelling being mainly governed by strong electrostatic repulsions of the protonated amine groups. To understand how different DF could impact dPG-NH<sub>2</sub>-mediated siRNA delivery, we next performed MD simulations for the binding of the tested DNA molecules to the different dPG-NH<sub>2</sub> analogues (pH 7.4 and 9.4 mM NaCl). The relevant results are shown in Figure 2, while the corresponding numerical values are listed in the lower part of Table 2. For a rigorous quantification of the interaction between the different dPG-NH<sub>2</sub> molecules and DNA, we assessed the effective free energy of binding  $\Delta G_{bind}^{eff}$  for each dPG-NH<sub>2</sub>/DNA complex, that is the contribution to binding yielded by the dPG-NH<sub>2</sub> branches in constant and productive contact with DNA.<sup>35-41,42,24, 43</sup> Accordingly, we precisely identified all dPG-NH<sub>2</sub> branches involved in nucleic acid binding ( $N_{eff}$ ), and their individual contribution toward the overall binding energy was estimated by a *per-residue* free energy decomposition technique.<sup>44</sup>

**Table 2.** Properties of dPG-NH<sub>2</sub> analogues obtained from molecular modeling.

	dPG-NH <sub>2</sub> 10%	dPG-NH <sub>2</sub> 30%	dPG-NH <sub>2</sub> 50%	dPG-NH <sub>2</sub> 90%
$\Phi$ (nm) <sup>a</sup>	4.0 ± 0.4	4.4 ± 0.5	4.8 ± 0.3	5.7 ± 0.3
$N_{eff}$ (-) <sup>b</sup>	5	11	15	16
$\Delta G_{bind}^{eff}$ (kcal/mol) <sup>c</sup>	-35.1 ± 2.9	-82.5 ± 5.1	-171.0 ± 5.6	-195.2 ± 8.1
$\Delta G_{bind}^{eff}/N_{eff}$ (kcal/mol) <sup>d</sup>	-7.0 ± 0.6	-7.5 ± 0.8	-11.4 ± 0.4	-12.2 ± 0.5

<sup>a</sup> The first row reports the diameter  $\Phi$  of the four different dPG-NH<sub>2</sub> molecules predicted by atomistic simulation. The remaining properties refer to dPG-NH<sub>2</sub>/DNA complexes: <sup>b</sup>  $N_{eff}$  is the number of dPG-NH<sub>2</sub> branches efficiently involved in DNA binding, <sup>c</sup>  $\Delta G_{bind}^{eff}$  is the effective free energy of binding between dPG-NH<sub>2</sub> and DNA, and <sup>d</sup>  $\Delta G_{bind}^{eff}/N_{eff}$  highlights how strong each active contact is in binding DNA.

The first important result from these studies concerns the number of effective branches interacting with the nucleic acid (i.e.,  $N_{eff}$ ). As expected,  $N_{eff}$  is the smallest (5) for dPG-NH<sub>2</sub> 10%: Due to the low degree of hydroxyl (OH) substitution and statistical positioning of NH<sub>2</sub> charged groups (Figure 2, top left), there is a limited number

of protonated groups involved in binding DNA. Amine substitution for dPG-NH<sub>2</sub> 30% involves almost the complete external shell of the molecule and  $N_{eff}$  substantially increases to 11 (Figure 2, top right).

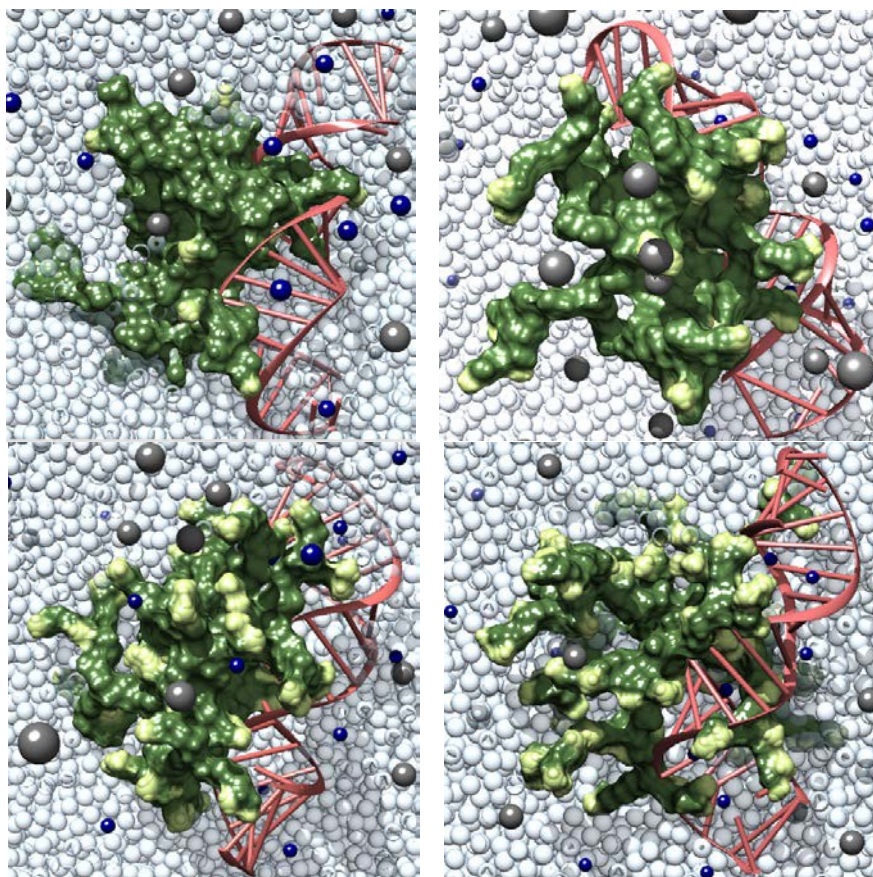


**Figure 2.** MD-equilibrated snapshots of the four dPG-NH<sub>2</sub> studied in complex with a 21-bp DNA. dPG-NH<sub>2</sub> analogues are depicted as a dark green surface with charged NH<sub>2</sub> groups highlighted in light green. The DNA chain is portrayed in a pale violet-red ribbon-ladder style. Cl<sup>-</sup>, Na<sup>+</sup> ions and water molecules are represented as dark grey, navy blue, and light blue spheres, respectively. (Top right panel) dPG-NH<sub>2</sub> 10%, (top left panel) dPG-NH<sub>2</sub> 30%, (bottom left panel) dPG-NH<sub>2</sub> 50%, (bottom right panel) dPG-NH<sub>2</sub> 90%.

Interestingly, higher DF (50% and 90%, respectively) do not induce a significant rise in the number of active contacts between dPG-NH<sub>2</sub> and DNA (15 and 16, respectively), which suggest that a threshold in binding efficiency has been achieved (Figure 2, bottom panels) for these molecules. These results are in complete agreement with the findings of the ethidium bromide displacement assay. Nevertheless, if we work out the effective binding energy for each active binding group with DNA (i.e.,  $\Delta G_{bind}^{eff}/N_{eff}$ ), we see that the affinity of each stable contact is much higher in dPG-NH<sub>2</sub> 50% and 90% than in dPG-NH<sub>2</sub> 30% (and 10%). This demonstrates that dPG-NH<sub>2</sub> 50% and 90% binding residues are more effective in binding DNA than lower amine-functionalized counterparts. To investigate in detail the nature of the intermolecular interactions steering the binding process, we deconvoluted

the enthalpic contribution to dPG-NH<sub>2</sub>/DNA binding  $\Delta H_{bind}^{eff}$  into its dispersive (nonpolar)  $\Delta E_{nonpol,tot}^{eff}$  and electrostatic (polar)  $\Delta E_{pol,tot}^{eff}$  components ( $\Delta H_{bind}^{eff} = \Delta E_{nonpol,tot}^{eff} + \Delta E_{pol,tot}^{eff}$ ) as shown in Figure 3.

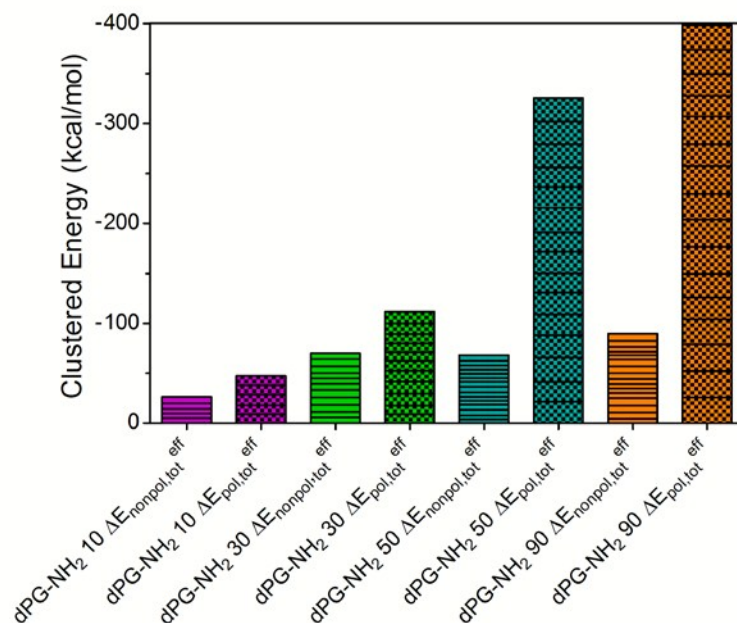


**Figure 3.** Decomposition of the effective binding enthalpy  $\Delta H_{bind}^{eff}$  on a *per-residue* effective basis into contribution of nonpolar ( $\Delta E_{nonpol,tot}^{eff} = \Delta E_{vdw,tot}^{eff} + \Delta E_{np,tot}^{eff}$ ) and polar ( $\Delta E_{pol,tot}^{eff} = \Delta E_{ele,tot}^{eff} + \Delta E_{GB,tot}^{eff}$ ) terms for each dPG-NH<sub>2</sub>/DNA complex.

From this analysis we found that, for both dPG-NH<sub>2</sub> 10% and 30%, both  $\Delta E_{pol,tot}^{eff}$  ( $\Delta E_{pol,tot}^{eff} = \Delta E_{ele,tot}^{eff} + \Delta E_{GB,tot}^{eff}$ ) and  $\Delta E_{nonpol,tot}^{eff}$  ( $\Delta E_{nonpol,tot}^{eff} = \Delta E_{vdw,tot}^{eff} + \Delta E_{np,tot}^{eff}$ ) almost equally contribute to binding. As the number of protonated groups per effective residue increases (dPG-NH<sub>2</sub> 50% and 90%), that is 2 and 3 positive charges per contacting group, the total polar term prevails. Moreover, each individual charge contribution is not merely additive but favorable synergistic, a prototypical phenomenon underlying multivalency. Addition of a third protonated group leads to an increased binding affinity for contacting residues (-11.4 kcal/mol for dPG-NH<sub>2</sub> 50% and -12.2 kcal/mol for dPG-NH<sub>2</sub> 90%, respectively). However, due to the distance of this charge from the nucleic acid, its contribution is substantially less effective than those exerted by the other protonated groups on the same residue.

### DLS and Zeta potential

The particle size in solution of four dPG-NH<sub>2</sub> analogues and the correlation of their surface charges ( $\zeta$ ) was studied using dynamic light scattering (DLS). According to the DLS measurements, the size of four dPG-NH<sub>2</sub> molecules in

aqueous solution (intensity-based distributions) was in the range of 6-14 nm. The volume-based distributions of dPG-NH<sub>2</sub> molecules ranged from 4 to 6 nm (see Table 1 and SI). The slight increase in the size of dPG-NH<sub>2</sub> analogues is in agreement with the result of our MD simulations presented in Table 2, which predict an increase in the size of polyamines, especially for those molecules with higher than 50% amine DF. The analysis of intensity-based size distribution of dPG-NH<sub>2</sub> analogues demonstrated the presence of some aggregations for all polyamines. However, considering the results of volume-, number-, and the intensity-based size distribution for dPG-NH<sub>2</sub> analogues, it can be concluded that these aggregation compromise only a small fraction of each sample (See SI for further results of size distributions).

**Table 3** : Physicochemical characteristics of dPG-NH<sub>2</sub> molecules/siRNA polyplexes at N/P ratio 5.

polyplex	Size		$\zeta$ (mV)
	d (nm)	Intensity %	
dPG-NH <sub>2</sub> 10%	130	99.6 %	1.5 ± 0.2
	19.15	0.4	
dPG-NH <sub>2</sub> 30%	164	83.5	10.3 ± 0.4
	12.8	10%	
dPG-NH <sub>2</sub> 50%	93	90%	8.6 ± 0.3
dPG-NH <sub>2</sub> 90%	96.9	98.7%	7.5 ± 0.3
	18	1.3	

Under the adopted experimental conditions, all dPG-NH<sub>2</sub> molecules were positively charged with an average charge of about 10 mV. Predictably, there is a slight increase in the positive charge of the polyamines as a consequence of the increased number of amine groups per dPG scaffold. DLS measurements were further applied to analysis the physicochemical properties of dPG-NH<sub>2</sub> molecules/siRNA polyplexes. At N/P ratio 5, these polyplexes showed a size between 90-130 nm (Figure 4). The surface charge of dPG-NH<sub>2</sub> analogues/siRNA at the same N/P ratio was slightly positive and in the case of dPG-NH<sub>2</sub> molecules with DF ≥ 30% was comparable (Table 3). As discussed above, both EthBr displacement assay and MD simulations provided evidence of stronger interactions between dPG-NH<sub>2</sub> 50% and 90% and genetic materials with respect to the counterparts with lower amine DF. We were further interested to explore the zeta potential ( $\zeta$ ) changes of dPG-NH<sub>2</sub> molecules upon pH variation over a biologically relevant range of values (i.e., 4-8). In general, the surface charge of dPG-NH<sub>2</sub> analogues is pH dependent and increases as pH drops. The  $\zeta$  value of all dPG-NH<sub>2</sub> analogues is highly positive over the measured range and progressively increases with decreasing pH from 8 to 4 (Figure 5). As expected,

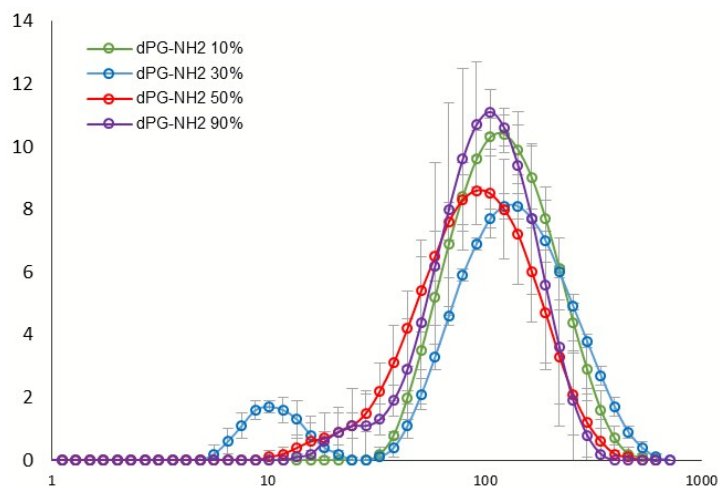


**Figure 4.** Size measurements (intensity distributions) of dPG-NH<sub>2</sub> analogues/siRNA polyplexes at N/P ratio 5.

higher numbers of amine groups per dPG unit reflect the higher values of the corresponding zeta potential. Interestingly, dPG-NH<sub>2</sub> 90%, which already has shown high potential for siRNA delivery,<sup>25</sup> exhibits the highest zeta potential compared to all other amine-functionalized dPGs at all measured pH points. According to these results, dPG-NH<sub>2</sub> analogues of 50% and 90% amine DF exhibit higher positive charges at lower pH values. High positive charges at pH values below physiological pH, can facilitate the endosomal release of polyplexes into cytosol through the proton sponge effect.<sup>45</sup>

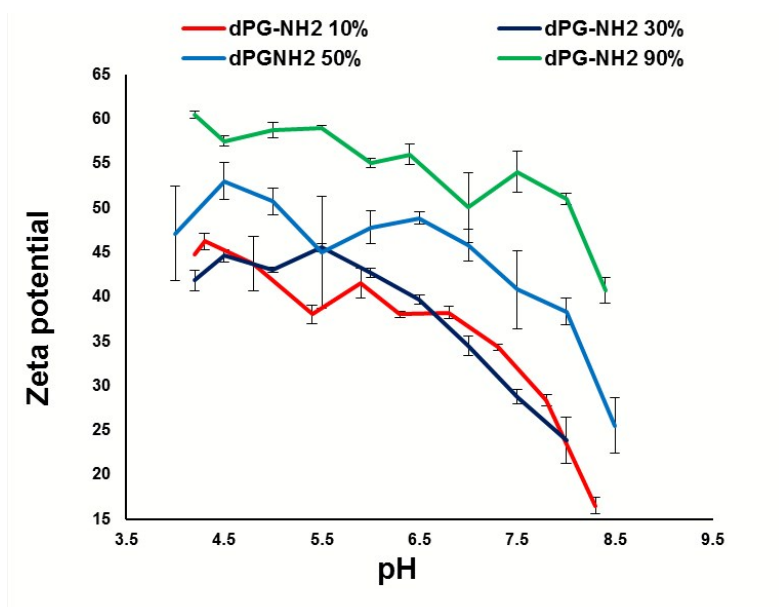


**Figure 5.** Zeta potential changes of dPG-NH<sub>2</sub> analogues over the pH range of 4 to 8.

### *In vitro* Transfection

After the study of the general physicochemical features related to gene binding with the 21-bp DNA, the performance of the dPG-NH<sub>2</sub> series for siRNA delivery was analyzed through the downregulation of ferrochelatase (FECH) in MDA-MB-231 cells. Protoporphyrin-IX (PpIX) is a fluorescent metabolite of the heme biosynthesis pathway, in which the FECH enzyme catalyzes the last step of the synthesis where the incorporation of iron into PpIX results in the heme formation. Downregulation of FECH, as a result of RNA interference (RNAi) machinery, leads to accumulation of PpIX and, consequently, an increase of PpIX fluorescence emission (Figure 6). To evaluate our dPG-NH<sub>2</sub> polyplexes regarding siRNA knockdown efficiency *in vitro*, we measured the fluorescence emission resulting from PpIX accumulation in MDA-MB-231 cells line. Earlier, we had established an *in vitro* model in which FECH downregulation corresponded directly to PpIX-dependent fluorescence emission enhancement.<sup>46</sup> We have shown by flow cytometry and confocal fluorescence microscopy that PpIX fluorescence emission is induced in a highly specific manner by silencing of FECH mRNA.<sup>27</sup> Moreover, it has been proved that carcinoma cells show a significant downregulation of FECH mRNA expression and decrease of enzyme activity.<sup>46</sup> Hence, MDA-MB-231 cells were treated with polyplexes of dPG-NH<sub>2</sub> analogues with either FECH or control siRNA.

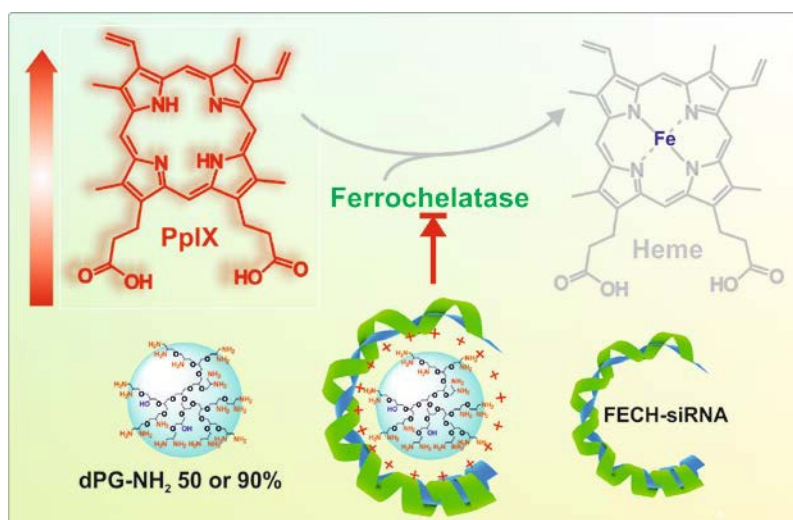


**Figure 6.** Downregulation of FECH by siRNA delivery using dPG-NH<sub>2</sub>s as carrier results in accumulation of PpIX fluorescence.

Prior to the silencing study cytotoxicity of different dPG-NH<sub>2</sub> polyplexes was evaluated on breast carcinoma MDA-MB-231 cells. N/P ratio of 5:1 with 10 pmol siRNA were analyzed since such condition showed to be optimal for silencing in our previous study.<sup>27</sup> In such conditions, polyplexes of dPG-NH<sub>2</sub> molecules with 30% and higher amine DF demonstrated moderate cytotoxic effects *in vitro* (Figure 7). We have previously observed a comparable trend

of cytotoxicity in U-937 cell line for dPG-NH<sub>2</sub> analogues with 30% and higher amine DF.<sup>28</sup> In line with previous findings for positively-charged nanovectors,<sup>47</sup> and dPG-NH<sub>2</sub> analogues of various amine DF,<sup>28</sup> the cytotoxicity of these molecules with  $\geq 30\%$  amine DF could sensibly be ascribed to the relatively high positive charge density on their surface.

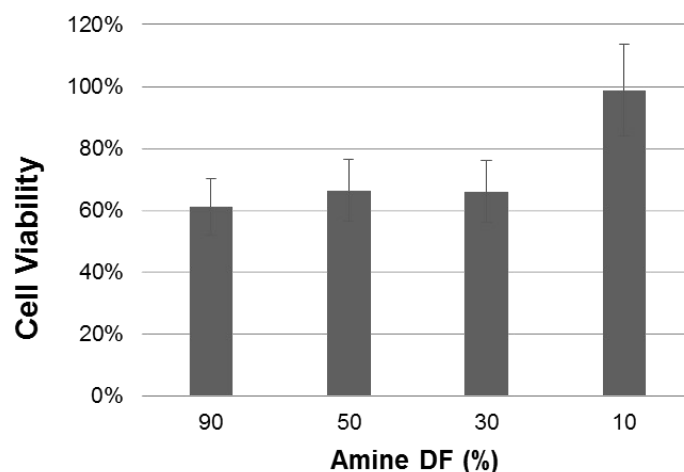


**Figure 7.** Cytotoxicity results of dPG-NH<sub>2</sub>/siRNA polyplexes on breast carcinoma cells MDA-MB-231. Polyplexes were prepared at the same concentration as in the *in vitro* silencing experiment (N/P ratio 5:1, with 10 pmol siRNA). There is a significant ( $p < 0.05$ ) difference between the viability of cells treated with polyplexes with 10% DF (column on the right side) and cells treated with another dPG-NH<sub>2</sub> (with 30% to 90% DF).

Treatment of MDA-MB-231 cells with polyplexes of FECH siRNA and dPG-NH<sub>2</sub> 10% or 30% resulted in low PpIX-fluorescence emission. In fact, the fluorescence intensities in these two cases were comparable to those of cells treated with polyplexes constructed with control siRNA and dPG-NH<sub>2</sub> 10% or 30% (fluorescence intensities  $1.2 \times 10^2$  to  $1.8 \times 10^2$ ). On the contrary, PpIX fluorescence emission after cell treatment with polyplexes of FECH siRNA and dPG-NH<sub>2</sub> 50% and 90% increased 32- and 78-fold, respectively. (Figure 8). These results clearly confirm the ability of dPG-NH<sub>2</sub> analogues with degrees of amine functionalization  $\geq 50\%$  on dendritic scaffold to knockdown FECH mRNA and induce a PpIX fluorescence emission *in vitro*.

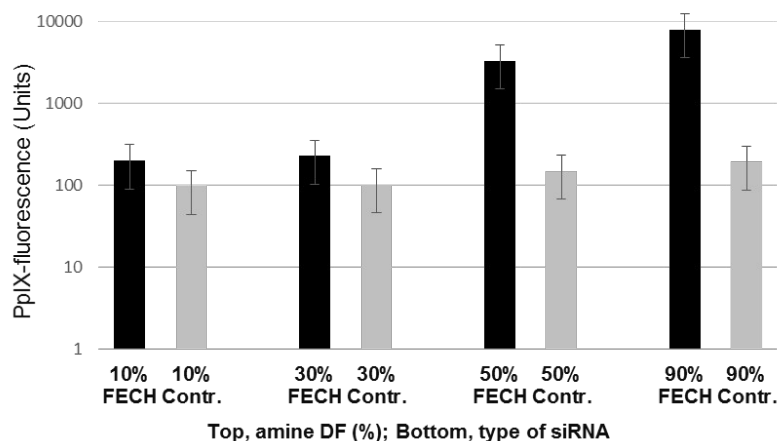


**Figure 8.** Flow cytometry analysis of PpIX-fluorescence in breast carcinoma cells MDA-MB-231. Cells were treated with FECH and a negative control siRNA N3. Y-axis, PpIX-fluorescence (Note logarithmic scale); X-axis, different dPG-NH<sub>2</sub> analogues incubated with FECH siRNA (black columns) or control siRNA (gray columns). There is a significant ( $p < 0.05$ ) difference between the PpIX-fluorescence of cells treated with polyplexes containing FECH siRNA with 10% or 30% DF and cells treated with another dPG-NH<sub>2</sub> (50% and 90% DF). There is also a significant ( $p < 0.05$ ) difference between the PpIX-fluorescence of cells treated with FECH siRNA dPG-NH<sub>2</sub> with 90% and 50% DF and control siRNA dPG-NH<sub>2</sub> polyplexes.

### ***In vivo* Transfection**

To further examine our dPG-NH<sub>2</sub> nanocarriers regarding their transfection efficiency *in vivo*, we chose a facile and straightforward method, namely, fluorescence imaging. This method allows easy screening of efficient siRNA vectors by just analyzing the intensities of fluorescence images. As aforementioned, siRNA-based inhibition of ferrochelatase results in blockage of heme-synthesis, which, in turn, allows the detection of a xenotransplanted human tumor due to the consequent, endogenous accumulation of PpIX. Here, the potential of various dPG-NH<sub>2</sub> polyplexes for *in vivo* FECH silencing was assessed applying the same methodology. Therefore, dPG-NH<sub>2</sub> polyplexes were injected intratumorally in xenografted mice twice with a 4-day break between the two treatments. Each treatment group comprised three animals. Since we have found that PpIX accumulation can be enhanced by addition of the heme-synthesis anabolite 5-aminolevulinic acid (5-ALA),<sup>46</sup> a low concentration of 5-ALA (10 mg/kg body weight) was also applied intratumorally on the day of the fluorescence measurement. As can be seen from Figure 9, the results show almost no PpIX-dependent fluorescence increase as a result of the 5-ALA introduction. In contrast, after treatment of the mice with dPG-NH<sub>2</sub> 50%/FECH-siRNA polyplexes followed by a single dose of 5-ALA (at the same concentration), fluorescence within the xenografts started to increase within 2 h after the injection and reached its highest level after 3 h (Figure 9). Also, as it was anticipated, no PpIX-fluorescence emission was observed within the tumor xenografts after injection of the dPG-NH<sub>2</sub> 10%/ and 30%/

FECH-siRNA polyplexes.

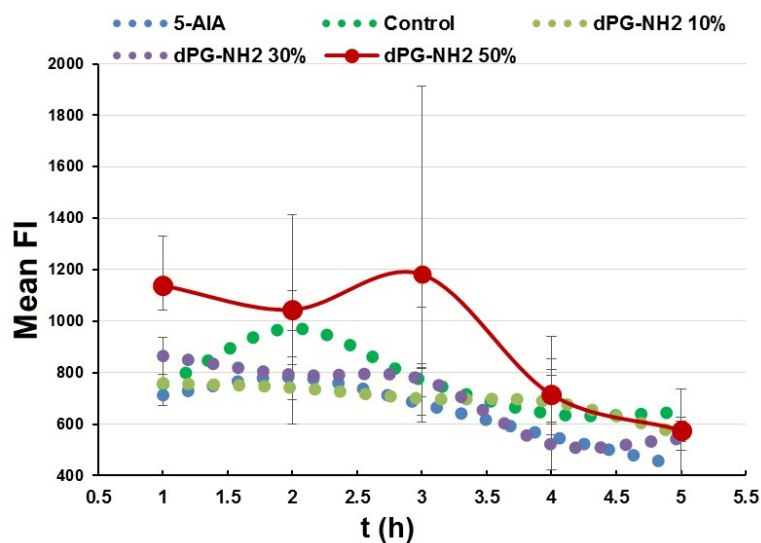


**Figure 9.** PpIX mean fluorescence intensities after introduction of dPG-NH<sub>2</sub> analogues FECH siRNA polyplexes over 5 h.

Moreover, the transplanted tumors clearly showed a local fluorescence signal after using dPG-NH<sub>2</sub> 50% as FECH siRNA vector (Figure 10). Although the fluorescence intensity for the dPG-NH<sub>2</sub> 50%/FECH siRNA polyplexes in this study was lower than that of dPG-NH<sub>2</sub> 90% in our previous study,<sup>27</sup> the results of both studies jointly suggest a minimum of 50% amine DF per dPG unit as a requirement for efficient siRNA knockdown both *in vitro* and *in vivo*.

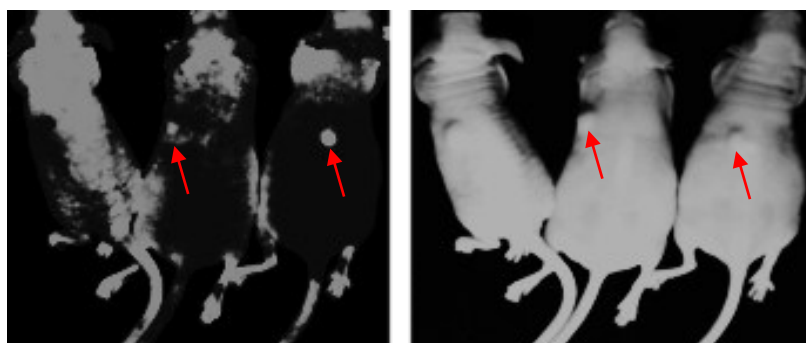


**Figure 10.** Fluorescence images of xenografted tumors in nude mice transfected by intratumoral injection of dPG-NH<sub>2</sub> 50% polyplexes. Unspecific staining on the back of the left mouse occurred due to the diet or contact of mouse skin with 5-ALA within the litter. Fluorescence was not found in the tumors of other groups. Right side, light image showing the xenografted tumors; Left side, fluorescence image, arrows point to the tumors which show PpIX-fluorescence.

## Experimental part

### Materials

The chemicals were of analytical grade and were purchased from Sigma-Aldrich (Germany), Acros (Germany), and Fischer scientific (Germany). Unless otherwise mentioned, all chemicals were used as received from the suppliers and without further purification. Dialysis tubing with MWCO of 2000 g mol<sup>-1</sup> was purchased from Sigma-Aldrich. FECH siRNA and control siRNA N3 were purchased from Riboxx Life Sciences (Freiburg, Germany). 5-aminolevulinic acid (5-ALA) was also purchased from Sigma-Aldrich (Munich, Germany). Dulbecco's Modified Eagle's Medium, fetal calf serum, phosphate buffered saline (PBS), antibiotics, and glutamine were from GIBCO (Eggenstein, Germany). Dharmafect transfection reagent was delivered from Thermo Scientific (Bremen, Germany). All water used for buffer preparations and biological studies was of Millipore quality (resistivity ~ 18 MΩ cm<sup>-1</sup>, pH = 5.6 ± 0.2). For EthBr displacement assay a 21-bp DNA (Lamin A/C) from Qiagen was used. The sequence of DNA was as follows (5'-CTGGACTTCCAGAAGAACATT-3').

### Methods

#### Synthesis of dPG-NH<sub>2</sub> analogues

dPG with average molecular weight of 10.6 kDa (PDI = 1.4) and 52% degree of branching (See SI for DB calculation) was prepared following literature procedures.<sup>48,49</sup> Synthesis of dPG-NH<sub>2</sub> analogues was executed according to a three-step protocol.<sup>50</sup> The through synthetic procedure of dPG-NH<sub>2</sub> with various functionalization degree, has been reported by our group (For synthetic details see SI).<sup>28</sup>

#### Binding Studies

EthBr displacement assay was used to evaluate the binding affinity of dPG-NH<sub>2</sub> analogues towards nucleic acids. The experimental procedure was performed according to a previously published assay.<sup>51</sup> Fluorescence spectroscopy measurements were carried out with a JASCO FP-6500 spectrofluorometer. Therefore, a stock solution of EthBr (8 μM) and DNA (0.2 mM) were prepared. Solutions of EthBr (10 nmol) and DNA (30 nmol) in HEPES buffer (2 mM, 10 μM EDTA and 9.4 mM NaCl, pH 7.2) were incubated at room temperature for 15 min. Different concentrations of each dPG-NH<sub>2</sub> corresponding to different N/P ratios were added to a mixture of EthBr

and DNA and incubated for additional 30 min. Fluorescence intensities were measured and compared to the fluorescence intensity of DNA and EthBr alone.

### **Dynamic light scattering (DLS), Zeta Potential, and Titration Studies**

Size and zeta potential of dPG-NH<sub>2</sub> analogues and their corresponding polyplexes with FECH siRNA were measured by a Zetasizer (NanoZS) (Malvern Instruments, Malvern, UK) with an integrated 4 mW He-Ne laser ( $\lambda = 633$  nm) at 25 °C with detection angle of 173°. Practically, dPG-NH<sub>2</sub> solutions were prepared shortly before the measurements. After dissolving 5 mg of dry polyamine in 1 mL aqueous phosphate buffer (10 mM, pH 7.4) DLS results were recorded. The same samples were analyzed afterwards for zeta potential. Surface charge measurements were carried out using folded capillary cells (DTS 1060). For each sample, measurements were repeated at least three times.

Zeta potential changes of dPG-NH<sub>2</sub> analogues in aqueous solution over a pH range of (4-8) were studied using a MPT-2 multipurpose autotitrator (Malvern Instruments, Malvern, UK). In each case, a solution of dPG-NH<sub>2</sub> in ultrapure water with a concentration of 1 mg mL<sup>-1</sup> of polymer was prepared. 1 mg of each polymer corresponded to a concentration of 1.3 mM, 4 mM, 6.6 mM, and 12 mM of amines on dPG-NH<sub>2</sub> with 10, 30, 50, and 90% DF, respectively. Titration was started at pH 8 and continued up to pH 4. A 1 M solution of NaOH and three 1 M, 0.1 M, and 0.01 M solutions of HCl were used as titrants. For preparation of the titrants ultrapure water was used. The performance of the pH probe was checked by calibration before each titration session. For measuring the size and zeta potential ( $\zeta$ ) of dPG-NH<sub>2</sub> analogues/siRNA polyplexes, stock solutions of different dPG-NH<sub>2</sub> molecules (1 mg in 5 mL) and siRNA (40  $\mu$ M) were prepared in ultrapure water. Appropriate amount of each dPG-NH<sub>2</sub> was taken and mixed with 3.3  $\mu$ L (5 nmol phosphate) siRNA solution. The mixtures were then diluted to 100  $\mu$ L and incubated for 45 min at rt. These mixture were next subjected to DLS measurements. The same solution was taken and diluted with 0.9 mL phosphate buffer solution (10 mM, pH 7.4). The polyplexes were subjected to zeta potential measurements and the measurements were repeated at least three times.

### **Cytotoxicity Assay**

The number of viable cells was examined using the Calcein-AM method (life technologies, USA). According to this method, non-fluorescent calcein AM can be converted to a green-fluorescent calcein after acetoxymethyl ester hydrolysis by intracellular esterases only in viable cells. Briefly, breast carcinoma cells MDA-MB-231 were seeded

at a cell density of 200000 cells/well in triplicate in 6-well plates (Sarstedt, 51588 Nümbrecht, Germany) and cultivated for 24 hours. Subsequently, dispersions of the different dPG-NH<sub>2</sub> were added for 48h. Then, the cells were detached by trypsin treatment, the cell number was counted, and the cell morphology was documented using a Cellometer Vision device (Nexcelom, Lawrence, MA). After washing cells twice with PBS, 1 mL Calcein-AM-solution (1 $\mu$ M) was added to 100,000 cells. After mixing, cells (100  $\mu$ L per well) were pipetted into a 96-well microplate and incubated for 30 minutes at 37 °C. Then, the number of viable cells was determined by assessing the calcein fluorescence using a Fluostar Omega BMG LabTech (Ortenberg, Germany) fluorescence plate reader with an excitation at  $\lambda = 495$  nm and an emission at  $\lambda = 535$  nm.

### Transient FECH siRNA transfection of breast tumor cells

MDA-MB-231 cells, originally derived from a mammary carcinoma (ATCC HTB-26), were grown in Dulbecco's modified Eagle's medium (DMEM) supplemented with 10 % FBS, 2 mM glutamine, 0.6  $\mu$ g mL<sup>-1</sup> penicillin (equivalent to 100 units), and 0.1 mg mL<sup>-1</sup> streptomycin. For silencing FECH, the following sequence of the FECH siRNA was used: 5'- gaauauccucuugguuccg -3'. This sequence covers the FECH mRNA, transcript variant 1, with accession NM\_001012515.1 and was used before.<sup>27</sup> The negative control N3 siRNA has been validated and shown to ensure minimal nonspecific effects on gene expression and phenotype.<sup>52</sup> FECH mRNA expression of MDA-MB-231 cells is about 2.3 times higher than that of breast carcinoma cells MDA-MB-435 cells which have been used before.<sup>33,35</sup>

For both *in vitro* and *in vivo* experiments, siRNA was complexed with dPG-NH<sub>2</sub> analogues at 5:1 N/P ratio (the ratio between amino groups on dPG-NH<sub>2</sub> to the phosphate groups of siRNA). Therefore, an appropriate amount of each dPG-NH<sub>2</sub> (with 10% to 90% DF) was dissolved in PBS. For transfection, breast carcinoma cells MDA-MB-231 were seeded at a cell density of 200,000 cells/well in a 6-well plate and cultivated for 24 hours. Dispersions of dPG-NH<sub>2</sub> analogues in PBS were taken, mixed with 10 pmol FECH or control siRNA and incubated for 15 min at 37°C. Subsequently, RPMI medium was added to all siRNA/dPG-NH<sub>2</sub> solutions to a final volume of 100  $\mu$ L and a final siRNA concentration of 1 nM. Cells were incubated with siRNA/dPG-NH<sub>2</sub> complexes in RPMI with FCS for 48 hours at 37°C. Afterwards, cells were detached by trypsin treatment, cell number was counted and cell morphology was documented using a Cellometer Vision device (Nexcelom, Lawrence, MA). Subsequently, the cells were treated with 0.2 mM 5-ALA in RPMI with FCS for 3 h at 37 °C. The resulting PpIX-fluorescence was

detected with a BD Fortessa flow cytometer (BD Biosciences, San Jose, USA) at an excitation of 405 nm and an emission of 635 nm. All experiments were done in triplicate.

### ***In Vivo* Transfection**

All animal experiments were performed in accordance with relevant guidelines and regulations at the Experimental Pharmacology & Oncology Berlin-Buch GmbH (EPO GmbH). Human mammary carcinoma MDA-MB-231 cells ( $1 \times 10^7$  cells / mouse) were inoculated into the right flank of 6-7 week-old nude mice. Thereafter, the animals were kept for 2 weeks to allow the development of tumors up to a size of approximately  $3 \times 3$  mm. During this time animals were fed with a manganese deficient diet (ssniff® EF R/M manganese deficient, ssniff Spezialdiaeten GmbH, Soest) to reduce unspecific staining due to Mn-porphyrin structures. Tumor-bearing mice were randomized for the experimental studies. For *in vivo* intratumoral injection, a siRNA concentration of 238 nmol per kg of body weight was used. Accordingly, 20 nmol siRNA (920 nmol phosphate) was complexed with different amounts of four dPG-NH<sub>2</sub> analogues to obtain the same N/P ratio as *in vitro* studies. Injection of dPG-NH<sub>2</sub>/FECH-siRNA polyplexes into the xenograft tumors was carried out twice with a 4 day break between treatments. Three days later, the mice were treated with 10 mg kg<sup>-1</sup> body weight 5-ALA and the emission of PpIX fluorescence was determined over 5 hours.

### **Fluorescence Imaging**

Images were acquired using a fluorescence imaging system established at the Physikalisch-Technische Bundesanstalt, Berlin, Germany. PpIX fluorescence was excited with a power LED (Luxeon Star/O LED - Cyan Lambertian,  $\lambda_{\max} = 505$  nm, Lumileds Lighting, San Jose, CA, USA). A short pass filter ( $\lambda_{50\%} = 550$  nm) was used to cut longer wavelengths. PpIX-fluorescence was excited in a low absorbing Q-band to ensure light penetration through the skin. PpIX fluorescence intensity originating from transplanted tumor tissue was determined in relative quantities using an electron multiplied (EM) CCD-camera (Andor Technology plc., Belfast, UK). The custom-built pulsed light source was synchronized to the EMCCD camera to suppress illumination during charge transfer. Images were taken with a 50 mm Nikon objective covered by 2 long pass filters ( $\lambda_{50\%} = 600$  nm, Omega Optical inc., Brattleboro, USA) to suppress reflected excitation light. For quantification, we calculated the normalized fluorescence intensity of the main PpIX-fluorescence band at  $\lambda = 633$  nm. Three narcotized animals were measured at each time point. For anesthesia, a mixture of isofluran 2% and oxygen was used. For analysis

of fluorescence intensity, the regions of interest (ROIs) were placed over the tumor region and the 90 percentiles were determined.

### Molecular simulations

All simulations discussed in this work were carried out using the AMBER14 suite of programs<sup>53</sup> and performed with the GPU version of *pmemd* (*pmemd.cuda*) from AMBER14 on the EURORA GPU-CPU supercomputer (CINECA, Bologna, Italy). The AMBER ff12SB force field (FF)<sup>54</sup> and the new version of the Dreiding FF recently developed by the Goddard group and specifically optimized for dendritic molecules in water solutions<sup>55</sup> were employed for the 21 bp double-stranded DNA and the dPG-NH<sub>2</sub> molecules, respectively (See Figure 3 in SI for details). To build the 3D models of the dPG-NH<sub>2</sub> analogues/DNA complexes, the DNA chain was initially placed close to each dPG-NH<sub>2</sub> periphery. The resulting molecular pairs were subsequently energy minimized to yield starting structures devoid of substantial van der Waals overlaps. Each complex was then solvated with an appropriate number of TIP3P water molecules<sup>56</sup> extending at least 20 Å from the solute. A suitable number of Na<sup>+</sup> and Cl<sup>-</sup> counterions were added to neutralize the system and to mimic an ionic strength level of 9.4 mM. Each system was then subjected to a consolidated MD simulation protocol developed by our group.<sup>35-41</sup> Briefly, each solvated dPG-NH<sub>2</sub>/DNA complex was initially subjected to a combination of steepest descent and conjugate gradient energy minimization steps (50000 cycles), in order to relax close atomic distances. The optimized systems were then (i) gradually heated from 0 to 300 K using MD simulations in the canonical ensemble (NVT), which allowed a 20 ps interval per each 100 K with an integration step of 1 fs and employed a weak harmonic constraint (i.e., 20 (kcal/mol)/Å<sup>2</sup>) on the solute, and (ii) equilibrated for 10 ns at 300 K under Shake constraints<sup>57</sup> with a geometric tolerance of 5×10<sup>-4</sup> Å on all covalent bonds involving hydrogen atoms to prevent a substantial disruption of the hydrogen bond network. Further system equilibration was performed by carrying out 50 ns MD simulations in the isobaric-isothermal (NPT) ensemble and, starting from the last equilibrated frame, 50 ns of MD production runs were carried out on equilibrated systems again in the NPT ensemble for data collection and analysis.

The dPG-NH<sub>2</sub>/DNA free energy of binding ( $\Delta G_{bind}$ ) values were derived following our thoroughly validated ansatz<sup>35-41,34, 42, 58-61</sup> based on the Molecular Mechanics/Poisson Boltzmann Surface Area (MM/PBSA) approach<sup>62</sup> (see Supporting Information for full details). Energy values were averaged over 400 frames taken during equally spaced time intervals during the last 20 ns of the MD production steps. Normal mode analysis was carried out on a subset of 20 minimized MD snapshots evenly extracted from the relevant trajectory time frame used for energy

calculations. Finally, the identification of each dPG-NH<sub>2</sub> residue involved in DNA binding ( $N_{eff}$ ), and the corresponding effective free energy of binding values ( $\Delta G_{bind}^{eff}$ )<sup>35-41,42,24, 43</sup> were obtained performing a *per residue* binding free energy decomposition that exploited the MD trajectories of each given dPG-NH<sub>2</sub>/DNA ensemble.<sup>44</sup> This analysis was carried out using the MM/GBSA approach<sup>63</sup> and was based on the same snapshots used in the binding free energy calculations.

## Conclusion

A series of dPG-NH<sub>2</sub> analogues with increasing amine DF (10% to 90%) on a (10 kDa) dPG scaffold was successfully prepared. These dPG-NH<sub>2</sub> molecules were analyzed regarding their DNA binding properties. Additionally, the interaction of dPG-NH<sub>2</sub> analogues with a 21-bp DNA model was predicted using atomistic molecular dynamics simulations. Flow cytometry and *in vivo* fluorescence imaging techniques were employed to evaluate the transfection efficiency of dPG-NH<sub>2</sub> molecules both in cell lines and in tumor xenografted mice. The entire set of *in silico*, *in vitro*, and *in vivo* results definitely reveals that only those dPG-NH<sub>2</sub> analogues with 50% or higher DF could reach the cytoplasm and effectively silence the target FECH mRNA. The higher number of amine groups per dPG unit and thereby higher surface charge of dPG-NH<sub>2</sub> 50% and 90% seem to play an essential role in stronger interactions between nucleic acids and dPG-based polyamines. Additionally, the higher surface charge of dPG-NH<sub>2</sub> 50% and 90% particularly at pH values below physiological pH and its correlation with effective endosomal release, can possibly describe the more efficient transfection of dPG-based polyamines with  $\geq 50\%$  amine DF compared to analogues of lower DF. Although higher amine loading results in increased cytotoxicity, the silencing studies suggest that the multivalency related to the higher amount of amine functionalities play a crucial role on the efficient binding and delivery of siRNA. Thus, our combined theoretical/experimental approach allowed us to identify a minimum amine DF per dPG unit required for efficient siRNA interaction and transfection. Further biological studies are currently running to understand the role of dPG-NH<sub>2</sub>'s DF, molecular weight, and surface decoration in cellular uptake and endosomal release of their corresponding polyplexes.

## Acknowledgements

Authors would like to thank BMBF (Bundesministerium für Bildung und Forschung) within the Biotransporter project (project number: 13N11536), the SFB 765, and the Wilhelm Sander Stiftung, München, Germany for

financial support. We thank COST Network TD0802 (Dendrimers in Biomedicine) for supporting networking within this project. Furthermore, Dr Pamela Winchester is thanked for careful proofreading of this manuscript.

## References

1. P. S. Ramachandran, M. S. Keiser and B. L. Davidson, *Neurotherapeutics*, 2013, **10**, 473-485.
2. J. F. Guo, J. C. Evans and C. M. O'Driscoll, *Trends in Molecular Medicine*, 2013, **19**, 250-261.
3. D. V. Morrissey, J. A. Lockridge, L. Shaw, K. Blanchard, K. Jensen, W. Breen, K. Hartsough, L. Machemer, S. Radka, V. Jadhav, N. Vaish, S. Zinnen, C. Vargeese, K. Bowman, C. S. Shaffer, L. B. Jeffs, A. Judge, I. MacLachlan and B. Polisky, *Nature Biotechnology*, 2005, **23**, 1002-1007.
4. A. Ptasznik, Y. Nakata, A. Kalota, S. G. Emerson and A. M. Gewirtz, *Nature Medicine*, 2004, **10**, 1187-1189.
5. K. Gavrillov and W. M. Saltzman, *The Yale journal of biology and medicine*, 2012, **85**, 187-200.
6. R. J. Christie, N. Nishiyama and K. Kataoka, *Endocrinology*, 2010, **151**, 466-473.
7. K. A. Whitehead, R. Langer and D. G. Anderson, *Nature Reviews Drug Discovery*, 2010, **9**, 412-412.
8. E. Wagner, *Biomaterials Science*, 2013, **1**, 804-809.
9. K. Singha, R. Namgung and W. J. Kim, *Nucleic Acid Therapeutics*, 2011, **21**, 133-147.
10. A. Akinc, A. Zumbuehl, M. Goldberg, E. S. Leshchiner, V. Busini, N. Hossain, S. A. Bacallado, D. N. Nguyen, J. Fuller, R. Alvarez, A. Borodovsky, T. Borland, R. Constien, A. de Fougères, J. R. Dorkin, K. N. Jayaprakash, M. Jayaraman, M. John, V. Kotliansky, M. Manoharan, L. Nechev, J. Qin, T. Racie, D. Raitcheva, K. G. Rajeev, D. W. Y. Sah, J. Soutschek, I. Toudjarska, H.-P. Vornlocher, T. S. Zimmermann, R. Langer and D. G. Anderson, *Nature Biotechnology*, 2008, **26**, 561-569.
11. O. M. Merkel and T. Kissel, *Journal of Controlled Release*, 2014, **190**, 415-423.
12. F. S. Mehrabadi, W. Fischer and R. Haag, *Current Opinion in Solid State & Materials Science*, 2012, **16**, 310-322.
13. Q. Wei, S. Krysiak, K. Achazi, T. Becherer, P.-L. M. Noeske, F. Paulus, H. Liebe, I. Grunwald, J. Dervede, A. Hartwig, T. Hugel and R. Haag, *Colloids and Surfaces B-Biointerfaces*, 2014, **122**, 684-692.
14. T. Rossow, J. A. Heyman, A. J. Ehrlicher, A. Langhoff, D. A. Weitz, R. Haag and S. Seiffert, *Journal of the American Chemical Society*, 2012, **134**, 4983-4989.
15. A. F. Hussain, H. R. Krueger, F. Kampmeier, T. Weissbach, K. Licha, F. Kratz, R. Haag, M. Calderon and S. Barth, *Biomacromolecules*, 2013, **14**, 2510-2520.
16. M. Calderon, P. Welker, K. Licha, I. Fichtner, R. Graeser, R. Haag and F. Kratz, *J. Controlled Release*, 2011, **151**, 295-301.
17. R. Haag and F. Kratz, *Angewandte Chemie-International Edition*, 2006, **45**, 1198-1215.
18. H. Frey and R. Haag, *Journal of biotechnology*, 2002, **90**, 257-267.
19. R. K. Kainthan, S. R. Hester, E. Levin, D. V. Devine and D. E. Brooks, *Biomaterials*, 2007, **28**, 4581-4590.
20. R. K. Kainthan and D. E. Brooks, *Biomaterials*, 2007, **28**, 4779-4787.
21. C. Scholz, P. Kos, L. Leclercq, X. Y. Jin, H. Cottet and E. Wagner, *Chemmedchem*, 2014, **9**, 2104-2110.
22. T. Frohlich, D. Edinger, R. Klager, C. Troiber, E. Salcher, N. Badgular, I. Martin, D. Schaffert, A. Cengizeroglu, P. Hadwiger, H. P. Vornlocher and E. Wagner, *Journal of Controlled Release*, 2012, **160**, 532-541.
23. K. Miyata, N. Nishiyama and K. Kataoka, *Chemical Society Reviews*, 2012, **41**, 2562-2574.
24. A. Barnard, P. Posocco, M. Fermeglia, A. Tschiche, M. Calderon, S. Pricl and D. K. Smith, *Organic & Biomolecular Chemistry*, 2014, **12**, 446-455.
25. P. Ofek, W. Fischer, M. Calderon, R. Haag and R. Satchi-Fainaro, *Faseb Journal*, 2010, **24**, 3122-3134.
26. W. Fischer, M. Calderon, A. Schulz, I. Andreou, M. Weber and R. Haag, *Bioconjugate Chemistry*, 2010, **21**, 1744-1752.
27. K. Wan, B. Ebert, J. Voigt, Q. Wang, Y. Dai, R. Haag and W. Kemmner, *Nanomedicine-Nanotechnology Biology and Medicine*, 2012, **8**, 393-398.
28. J. Khandare, A. Mohr, M. Calderón, P. Welker, K. Licha and R. Haag, *Biomaterials*, 2010, **31**, 4268-4277.
29. F. S. Mehrabadi, H. X. Zeng, M. Johnson, C. Schlesener, Z. B. Guan and R. Haag, *Beilstein Journal of Organic Chemistry*, 2015, **11**, 763-772.
30. P. Posocco, E. Laurini, V. Dal Col, D. Marson, K. Karatasos, M. Fermeglia and S. Pricl, *Current Medicinal Chemistry*, 2012, **19**, 5062-5087.
31. E. L. P. Posocco, V. Dal Col, D. Marson, L. Peng, D. K. Smith, B. Klajnert, M. Bryszewska, A. M. Caminade, J. P. Majoral, M. Fermeglia, K. Karatasos, S. Pricl, Multiscale modeling of dendrimers and dendrons for

- drug and nucleic acid delivery. *Dendrimers in Biomedical Applications*, RSC Publishing, Cambridge, U.K., and Editon edn., 2013, pp. 148-166.
32. S. Malhotra, H. Bauer, A. Tschiche, A. M. Staedtler, A. Mohr, M. Calderón, V. S. Parmar, L. Hoeke, S. Sharbati, R. Einspanier and R. Haag, *Biomacromolecules*, 2012, **13**, 3087-3098.
  33. A. Tschiche, A. M. Staedtler, S. Malhotra, H. Bauer, C. Boettcher, S. Sharbati, M. Calderon, M. Koch, T. M. Zollner, A. Barnard, D. K. Smith, R. Einspanier, N. Schmidt and R. Haag, *Journal of Materials Chemistry B*, 2014, **2**, 2153-2167.
  34. A. Barnard, P. Posocco, S. Pricl, M. Calderon, R. Haag, M. E. Hwang, V. W. T. Shum, D. W. Pack and D. K. Smith, *Journal of the American Chemical Society*, 2011, **133**, 20288-20300.
  35. X. Liu, C. Liu, E. Laurini, P. Posocco, S. Pricl, F. Qu, P. Rocchi and L. Peng, *Molecular Pharmaceutics*, 2012, **9**, 470-481.
  36. K. Karatasos, P. Posocco, E. Laurini and S. Pricl, *Macromolecular Bioscience*, 2012, **12**, 225-240.
  37. P. Posocco, X. Liu, E. Laurini, D. Marson, C. Chen, C. Liu, M. Fermeglia, P. Rocchi, S. Pricl and L. Peng, *Molecular Pharmaceutics*, 2013, **10**, 3262-3273.
  38. S. M. Bromfield, P. Posocco, M. Fermeglia, S. Pricl, J. Rodriguez-Lopez and D. K. Smith, *Chemical Communications*, 2013, **49**, 4830-4832.
  39. S. Kala, A. S. C. Mak, X. Liu, P. Posocco, S. Pricl, L. Peng and A. S. T. Wong, *Journal of Medicinal Chemistry*, 2014, **57**, 2634-2642.
  40. S. M. Bromfield, P. Posocco, M. Fermeglia, J. Tolosa, A. Herreros-Lopez, S. Pricl, J. Rodriguez-Lopez and D. K. Smith, *Chemistry-a European Journal*, 2014, **20**, 9666-9674.
  41. D. Marson, E. Laurini, P. Posocco, M. Fermeglia and S. Pricl, *Nanoscale*, 2015, **7**, 3876-3887.
  42. X. Liu, J. Zhou, T. Yu, C. Chen, Q. Cheng, K. Sengupta, Y. Huang, H. Li, C. Liu, Y. Wang, P. Posocco, M. Wang, Q. Cui, S. Giorgio, M. Fermeglia, F. Qu, S. Pricl, Y. Shi, Z. Liang, P. Rocchi, J. J. Rossi and L. Peng, *Angewandte Chemie-International Edition*, 2014, **53**, 11822-11827.
  43. S. M. Bromfield, P. Posocco, C. W. Chan, M. Calderon, S. E. Guimond, J. E. Turnbull, S. Pricl and D. K. Smith, *Chemical Science*, 2014, **5**, 1484-1492.
  44. A. Onufriev, D. Bashford and D. A. Case, *Journal of Physical Chemistry B*, 2000, **104**, 3712-3720.
  45. O. Boussif, F. Lezoualc'h, M. A. Zanta, M. D. Mergny, D. Scherman, B. Demeneix and J. P. Behr, *Proceedings of the National Academy of Sciences of the United States of America*, 1995, **92**, 7297-7301.
  46. W. Kemmer, K. Wan, S. Ruettinger, B. Ebert, R. Macdonald, U. Klamm and K. T. Moesta, *Faseb Journal*, 2008, **22**, 500-509.
  47. D. Fischer, Y. X. Li, B. Ahlemeyer, J. Kriegelstein and T. Kissel, *Biomaterials*, 2003, **24**, 1121-1131.
  48. A. Sunder, R. Hanselmann, H. Frey and R. Mulhaupt, *Macromolecules*, 1999, **32**, 4240-4246.
  49. A. Sunder, R. Mulhaupt, R. Haag and H. Frey, *Macromolecules*, 2000, **33**, 253-254.
  50. M. Kramer, J. F. Stumbe, G. Grimm, B. Kaufmann, U. Kruger, M. Weber and R. Haag, *Chembiochem*, 2004, **5**, 1081-1087.
  51. M. A. Kostianen, D. K. Smith and O. Ikkala, *Angewandte Chemie-International Edition*, 2007, **46**, 7600-7604.
  52. L. Cottone, A. Capobianco, C. Gualteroni, C. Perrotta, M. E. Bianchi, P. Rovere-Querini and A. A. Manfredi, *International Journal of Cancer*, 2015, **136**, 1381-1389.
  53. V. B. D.A. Case, J. T. Berryman, R. M. Betz, Q. Cai, D. S. Cerutti, T. E. Cheatham III, T. A. Darden, R. E. Duke, H. Gohlke, A. W. Goetz, S. Gusarov, N. Homeyer, P. Janowski, J. Kaus, I. Kolossváry, A. Kovalenko, T. S. Lee, S. LeGrand, T. Luchko, R. Luo, B. Madej, K. M. Merz, F. Paesani, D. R. Roe, A. Roitberg, C. Sagui, R. Salomon-Ferrer, G. Seabra, C. L. Simmerling, W. Smith, J. Swails, R. C. Walker, V. Wang, R. M. Wolf, X. Wu and P. A. Kollman, *AMBER 14*, **2014**, University of California, San Francisco.
  54. W. D. Cornell, P. Cieplak, C. I. Bayly, I. R. Gould, K. M. Merz, D. M. Ferguson, D. C. Spellmeyer, T. Fox, J. W. Caldwell and P. A. Kollman, *Journal of the American Chemical Society*, 1996, **118**, 2309-2309.
  55. Y. Liu, V. S. Bryantsev, M. S. Diallo and W. A. Goddard, III, *Journal of the American Chemical Society*, 2009, **131**, 2798-+.
  56. W. L. Jorgensen, J. Chandrasekhar, J. D. Madura, R. W. Impey and M. L. Klein, *Journal of Chemical Physics*, 1983, **79**, 926-935.
  57. J. P. Ryckaert, G. Ciccotti and H. J. C. Berendsen, *Journal of Computational Physics*, 1977, **23**, 327-341.
  58. P. Posocco, M. Ferrone, M. Fermeglia and S. Pricl, *Macromolecules*, 2007, **40**, 2257-2266.
  59. G. M. Pavan, P. Posocco, A. Tagliabue, M. Maly, A. Malek, A. Danani, E. Ragg, C. V. Catapano and S. Pricl, *Chemistry-a European Journal*, 2010, **16**, 7781-7795.
  60. S. P. Jones, N. P. Gabrielson, C.-H. Wong, H.-F. Chow, D. W. Pack, P. Posocco, M. Fermeglia, S. Pricl and D. K. Smith, *Molecular Pharmaceutics*, 2011, **8**, 416-429.

61. D. J. Welsh, P. Posocco, S. Pricl and D. K. Smith, *Organic & Biomolecular Chemistry*, 2013, **11**, 3177-3186.
62. J. Srinivasan, T. E. Cheatham, P. Cieplak, P. A. Kollman and D. A. Case, *Journal of the American Chemical Society*, 1998, **120**, 9401-9409.
63. M. Feig, A. Onufriev, M. S. Lee, W. Im, D. A. Case and C. L. Brooks, *Journal of Computational Chemistry*, 2004, **25**, 265-284.